Available online at www.sciencedirect.com
ScienceDirect
Astroparticle Physics 28 (2007) 216–231
Astroparticle Physics
www.elsevier.com/locate/astropart

Using stars to determine the absolute pointing of the fluorescence detector telescopes of the Pierre Auger Observatory

For the Auger Collaboration
Cinzia De Donato [a,*], Michael Prouza [b,c], Federico Sanchez [d], Marcos Santander [e], Daniel Camin [a], Beatriz Garcia [e], Valerio Grassi [a], Jiří Grygar [c], Miroslav Hrabovský [c], Jan Řídký [c], Petr Schovánek [c], Petr Trávníček [c]

[a] *Physics Department of the University and INFN, Milano, Italy*
[b] *Department of Physics, Columbia University, New York, USA*
[c] *Institute of Physics, Academy of Sciences of the Czech Republic, Prague, Czech Republic*
[d] *Dep. Altas Energias, Inst. de Ciencias Nucleares, Universidad Nacional Autonoma de Mexico, Mexico, DF, CP04510, Mexico*
[e] *Universidad Tecnologica Nacional (UTN), Regional Mendoza and San Rafael, Mendoza, Argentina*

Received 3 July 2006; received in revised form 23 April 2007; accepted 22 May 2007
Available online 26 May 2007

Abstract

We describe in this paper two methods to accurately determine the absolute pointing of the fluorescence detector (FD) telescopes of the Pierre Auger Observatory. Our aim is to provide reliable and precise procedures to check and monitor the absolute telescope's pointing and its long-term stability during the whole life of the project, estimated to be about 20 years.

The two methods described, called "single pixel method" and "star track method", are based on the FD capability to be sensitive to signals left by stars traversing the telescope field of view. As the star positions in the sky are known with very high precision, the identification of the star signals provides a powerful tool to check the telescope alignment. We used data acquired during regular observation periods in 2004 and we demonstrated that the two methods presented in this paper provide compatible sets of pointing directions.

PACS: 96.40.−z; 96.40.Pq; 98.70.Sa

Keywords: Atmospheric fluorescence detector; Telescope's pointing; Long-term stability

1. The Pierre Auger Observatory

The Pierre Auger Observatory was conceived to investigate the nature of the ultra-high energy cosmic rays (UHECRs), in particular those with energy above 10^{18} eV. At this energy the integrated cosmic ray flux is rare, 1 particle/(km^2 year), leading to an experimental site that extends over a flat area of about 3000 km^2 at an altitude of 1400 m in Malargüe, Mendoza, Argentina.

So far the detection of ultra-high energy cosmic rays has been performed using two traditional and independent techniques, i.e. ground based surface detectors and fluorescence light detectors. These techniques measure, respectively, the particle density distribution at the ground and the longitudinal development of the shower's secondary particles generated when the primary cosmic ray arrives at the Earth's upper atmosphere. Both techniques, which allow an independent determination of the shower parameters and which were used separately in the past, are

* Corresponding author. Tel.: +39 0250317710.
E-mail address: cinzia.dedonato@mi.infn.it (C. De Donato).

0927-6505/$ - see front matter © 2007 Elsevier B.V. All rights reserved.
doi:10.1016/j.astropartphys.2007.05.008

combined for the first time in the Pierre Auger Observatory in a unique detector that allows a hybrid shower reconstruction, a distinctive and innovative feature of the experiment.

The Auger surface detector (SD) consists of 1600 water-Cherenkov tanks of 10 m^2 cross section and about 1.5 m high, separated from each other by 1.5 km in a triangular grid, that allow an accurate sampling of the shower lateral density distribution. The Auger fluorescence detector (FD), consisting of 24 telescopes sensitive to the UV light, measures the longitudinal development of the cosmic ray shower in the atmosphere above the Earth. This is done by detecting the fluorescence photons emitted isotropically by the nitrogen molecules excited by the shower's secondary particles propagating in the atmosphere [1–3]. Most of the fluorescence photons are emitted in the wavelength range between 300 and 400 nm for which the atmosphere is quite transparent, corresponding to an attenuation length of ≈15 km for a vertical beam of light. The fluorescence yield is ≈4 photons per electron traversing 1 m of atmosphere, mildly dependent on altitude and atmospheric temperature [4–7].

The coincident detection of a shower with both techniques, possible for about 10% of the events, facilitates the cross-calibration of the two detectors with a consequent reduction of the systematic errors. In order to achieve high resolution in the hybrid reconstruction of a shower and for all comparisons with SD geometric reconstructions it is essential to know with great accuracy the pointing capabilities of the FD telescopes. The precise knowledge of the FD absolute pointing can be used to cross check the SD pointing and systematics matching the hybrid events on the basis of the ground reference frame. A powerful tool to determine the alignment of the telescope, with the highest reachable accuracy, is the identification of signals left by stars traversing the field of view of the telescope, as it was also done at the HiRes Fly's Eye cosmic ray experiment [8]. Two new methods to determine the absolute telescope pointing were developed independently for the purposes of the Pierre Auger Observatory. In this work, these two methods are described and applied to the data acquired by the Observatory. The results obtained establish the validity of both our methods.

A detailed description of the Observatory and the performance of the hybrid detector prototype is given in [9,10].

1.1. The fluorescence detector

The FD comprises four sites located at the periphery of the SD array and overlooking it (Fig. 1). The FD sites are: Los Leones (LL), Coihueco (CO), Los Morados (LM) and Loma Amarilla (LA). Each FD site consists of a building with six sections, called *bays*,[1] each one containing a telescope sensitive to UV photons. The focal surface of the telescopes consists of a rigid and spherical aluminium piece (the camera) in which there are installed 440 photomultiplier tubes (PMTs), Photonis XP3062, arranged in a 20×22 array [11]. The PMTs have a semi-transparent bialcaline (SbKCs) photocathode of hexagonal shape and a quantum efficiency QE > 25% in the spectral band 350–450 nm. A UV transmitting filter (Schott M-UG6 glass sheets) installed in the 2.2 m diameter aperture improves the signal-to-noise ratio [12,13]. A spherical mirror with an area of 3.5 m × 3.5 m, a radius of curvature of 3.4 m and 1.743 m focal distance, as well as a corrector ring installed in the periphery of the aperture, complete the optical components. Each FD telescope has a field of view of 30° in azimuth and 28.6° in elevation. The main elements of the telescopes are shown in Fig. 2.

The telescope incorporates Schmidt optics to reduce the optical aberrations, where the aperture is defined by the circular diaphragm placed at the center of curvature of the spherical mirror. The great advantage of the optical system is the elimination of coma aberration owing to the addition of a corrector ring lens, keeping the light spot reflected on the camera at an angular size of 0.5° [14–16].

Each PMT is equipped with a Head Electronics unit (HE) which provides active bias. The active network improves linearity over the whole dynamic range compared to a standard passive base that would need to pass a current two times larger to obtain the same performance. The use of an active bias reduces the high voltage (HV) cost by 50% [17]. The PMT signal is sent to the front-end board (FEB) in differential mode where it is filtered and digitized at a 10 MHz sampling rate with 12 bit resolution.

2. FD background data

Two prototype FD telescopes were constructed at the initial stage of the project. The Head Electronics used in the first two prototypes incorporated the biasing network and a novel optical feedback system that reads the very slowly varying signal left by a star when it enters into the field of view (FOV) of a pixel. All 880 units were equipped with this *current monitor* [17,18]. On June 26, 2001 the first signal of Vega (Alpha Lyrae), Fig. 3, was clearly seen by the telescope at Los Leones [10,19].

After demonstrating the capability of the telescopes to be sensitive to even dim stars in the UV region, we incorporated a low-cost solution that returns the variance of the baseline fluctuation, which is proportional to the sky background light that also includes star signals. The measurement of the background light level, which is currently implemented in the Auger FD detectors, was extensively described in [20]. We will limit ourselves only to a short description here.

The method of the statistical current monitoring is based on an evaluation of the variance σ^2 of the background data. Because the incoming light flux follows Poisson statistics

[1] The bays are numbered counter-clockwise.

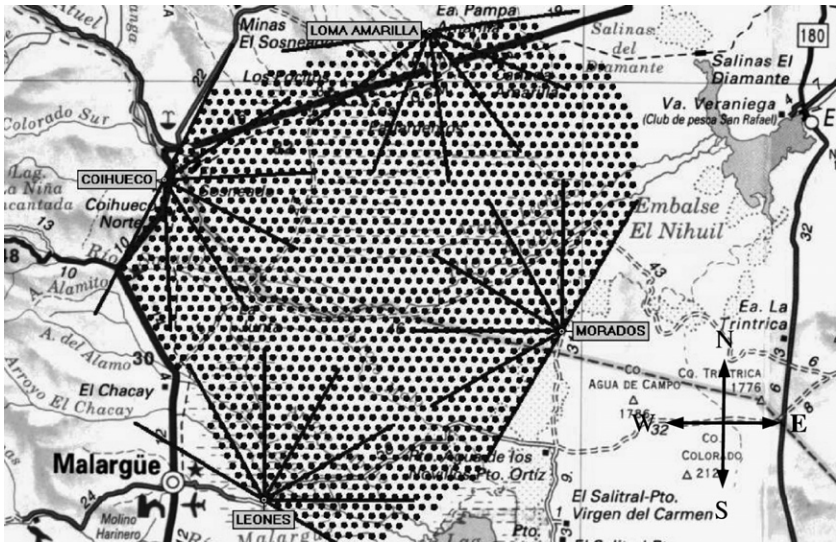

Fig. 1. Pierre Auger Observatory: the FD sites and the SD tanks (points) are shown.

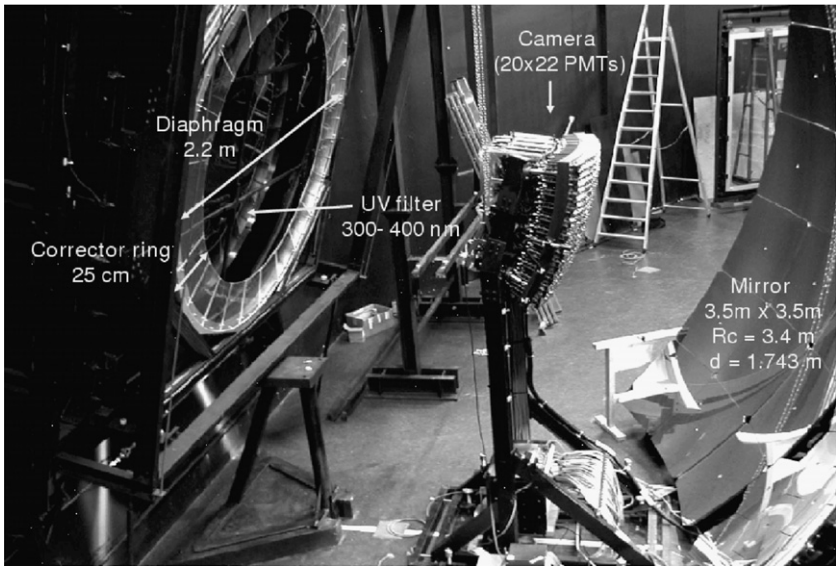

Fig. 2. Structure of a FD telescope. The aperture system consists of a diaphragm, a corrector ring and a UV filter. The other optical components are the mirror and the camera, this one comprising an array of 20×22 PMTs.

[20], the amplitude of the signal fluctuations is directly proportional to the intensity of the signal itself. Therefore, the signal variance sampled every 100 ns is recorded and then, from 65,535 such variance values, an average is computed and then stored. This statistical evaluation is done in parallel in the digital board (DB) by 4 field programmable gate array (FPGA) logic boards. Each FPGA handles in sequence 6 independent camera channels. Although the sampling could be faster, intrinsic limits of the system impose that the value for each pixel is stored every 30 s.

The variance analysis allows us to determine the incoming background light flux to the individual pixels. The typical photon flux at the southern site of the Auger Observatory in clear moonless night is of order 100 photons/m^2 deg^2 μs. A more detailed analysis of this sky background light level is done in [21] for data obtained from the Los Leones prototype telescopes. The signal left by stars is used in this work to determine the camera alignment because stars provide a reliable and stable coordinate system.

2.1. Camera geometry

A camera of 440 PMTs with a radius of 1.743 m (slightly larger than the standard focal length) is placed on the spherical focal surface of the mirror. The pixels are not regular hexagons; their sizes vary slightly over the focal surface to produce a constant angular dimension. The angular direction of each PMT center is given by the equations:

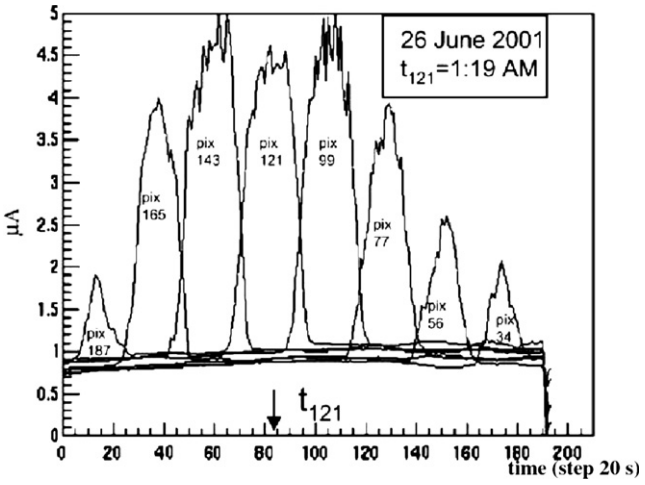

Fig. 3. Signals from the current monitor (μA) for adjacent pixels vs. time generated by the transit of Alpha Lyrae (Vega) in their FOV. The mean time of Vega's signal in the pixel 121, t_{121}, is indicated. The sampling time is 20 s.

$$\delta_{j,i} = \arcsin(\sin(\alpha_j + \alpha_m) \cdot \cos\beta_i), \quad (1)$$

$$\phi_{j,i} = \arcsin\left(\frac{\sin\beta_i}{\cos\delta_{j,i}}\right) + \phi_m, \quad (2)$$

where α_m and ϕ_m are the elevation and azimuth angles of the camera symmetry axis of telescope m in the local coordinate system, $\delta_{j,i}$ and $\phi_{j,i}$ are the elevation and azimuth angles in the sky of the pixel (j,i), and (α_j, β_i) are the angular direction of the pixel (j,i) in the coordinate system centered in the camera (Fig. 4).

As the camera has a rigid and defined structure, the pointing direction of the camera optical axis (which elevation angle differs from the camera symmetry axis by a known quantity) can be calculated from the pointing direction of each single pixel.

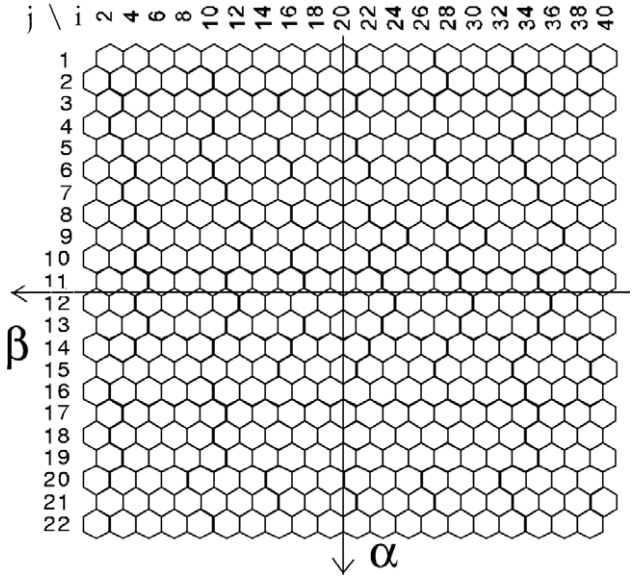

Fig. 4. 22×20 pixel matrix shown on the coordinate system centered on the camera (α, β).

2.2. Star images on the camera

The angular size of each PMT is about 1.5° for an inscribed circle into a PMT hexagon. The sensitive photocathode surface of the PMTs is smaller than its glass envelope and there are also mechanical reasons to leave some gaps between PMTs. The reflective edge-shaped plastic inserts, called *mercedes*, were applied to eliminate the insensitive areas between PMTs. Then, almost all the incident light is reflected onto some PMT and the focal surface is continuously covered. As the spot angular size fixed by the Schmidt optics is 0.5°, 1/3 the pixel size, we conclude that the FD pixel signal is ideally a trapezoidal current pulse whose rise and fall times are about 1/2 the flat top and that one star could influence the signal of up to 3 pixels simultaneously. In Fig. 5, an ideal signal shape is shown, to be compared with the real signals of Vega in Fig. 3.

The real signals show intensity fluctuations at the plateau[2]; the amplitude of these fluctuations, ranging from 10% to 20%, is due to the anisotropy of PMT photocathodes[3] [19], as well as to statistical fluctuations and to the intrinsic star *scintillations*, i.e. star intensity fluctuations due to the fast movements of atmospheric layers [22].

2.3. Light spots

The shape of the spot is not precisely circular. It is deformed by the shadowing of the camera body, by spherical aberration and by the use of a corrector ring on some telescopes.[4] More precisely, the spot deformation is more prominent for the cameras without a corrector ring. This spot shape deformation could result in a shift of the spot intensity center of up to 0.1° (Fig. 6). It is possible to model this star image displacement and then include this effect in the camera offset evaluation, as it was done within this work.

For the spot shape simulation we have used first a code developed within the collaboration which simulates the trajectories of light rays through different parts of the aperture according to the rules of geometrical optics. Because the optical system of the camera is not ideal, a sufficient number of rays (about 10^5 in our case) coming from a specified direction and covering the whole aperture will draw the spot shape. We run the program for 440 positions of pixels. For these resulting 440 spot shapes

[2] The signal plateau corresponds to the star image fully contained within the pixel.

[3] When the star traverses a pixel's FOV, it goes through regions of different cathode sensitivity and the signal could vary by up to 20%.

[4] During the analyzed periods only bays 3 and 4 both at Los Leones and Coihueco were equipped with corrector rings.

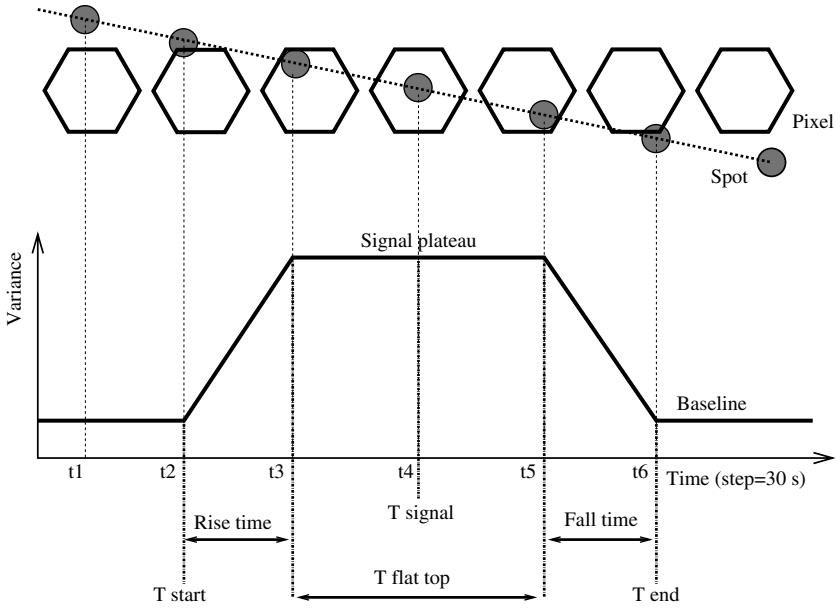

Fig. 5. Ideal signal shape. After identifying a star's signal in the variance data, a time T_{signal} is associated with it.

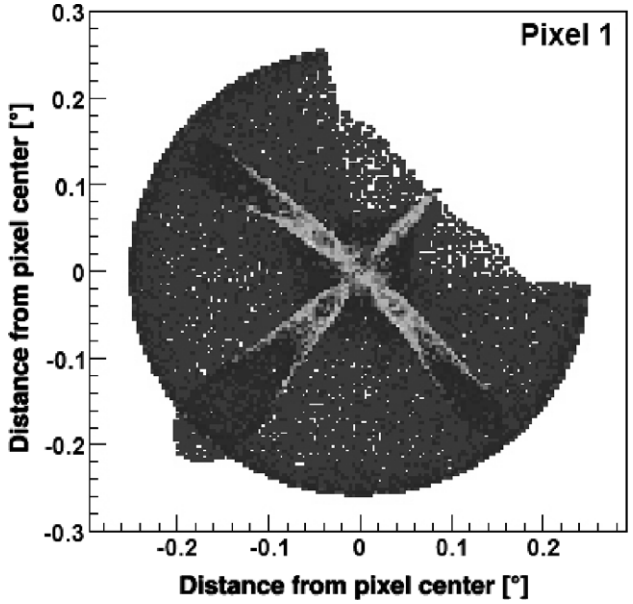

Fig. 6. Asymmetric spot shape for the pixel No. 1 (in the camera corner), as it was obtained using ray-tracing simulations of a point light source.

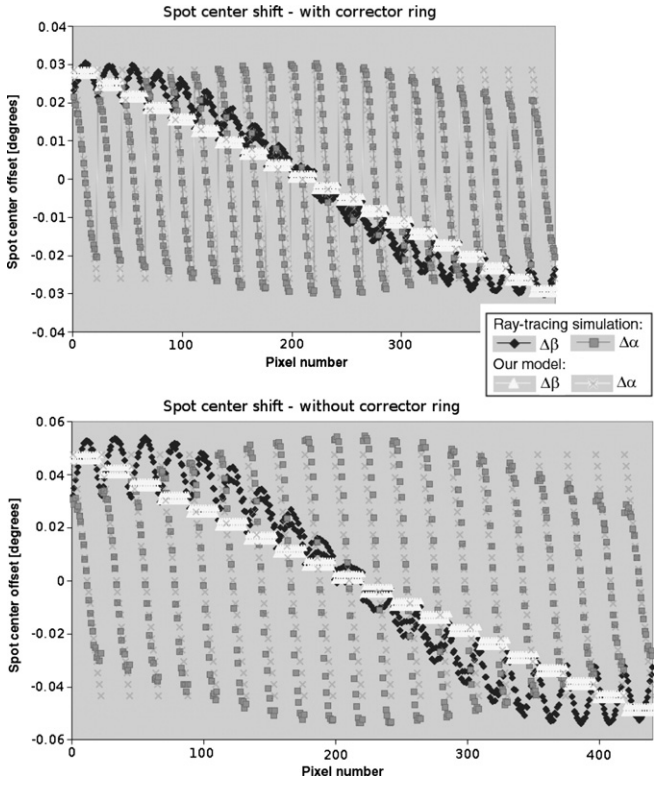

Fig. 7. Light spot intensity center. The plots show the offsets $\Delta\beta$ and $\Delta\alpha$ of the spot intensity center resulting from ray-tracing simulations for all the pixels of the camera. The same offsets are calculated by a simple numerical model and shown in the plots. For details see Section 2.3.

we computed the intensity center of each spot and compared its position with the position of the pixel center (the direction of the pixel center was the original direction of incident light rays). Then we plotted the resulting offsets (Fig. 7).

We realized that this behavior could be easily modeled under assumptions that the spot center offset is directly proportional to the distance from the camera center (in camera coordinates). Taking into account the spot shape deformation, the corrected position of the spot intensity center in horizontal β and vertical α coordinates (where β, α denote the angular distance from the camera center in degrees, as defined in Section 2.1) is given by:

- with corrector ring: $\beta' = 1.002\beta$, $\alpha' = 0.998\alpha$;
- without corrector ring: $\beta' = 1.0033\beta$, $\alpha' = 0.9967\alpha$.

The difference between our model and simulation results is less than 0.01° for the telescope with corrector ring and less than 0.02° without corrector ring, which we judge to be acceptable (Fig. 7).

2.4. Star positions on the sky

Stars are very suitable sources for camera alignment checks, because their positions in the sky are known with very high precision.

Horizontal coordinates (azimuth and elevation) of stars are obtained by standard coordinate transformations from equatorial coordinates (right ascension and declination), taking into account the Earth precession (an effect up to 0.1° for the analyzed period) and the atmospheric refraction. The shift in altitude due to the atmospheric refraction is about 0.3° for the lowest pixels and is dependent on the air pressure ρ and temperature T. We used the Meeus model [23] of atmospheric refraction with fixed pressure, 860 millibars, and with temperature T estimated on the basis of calendar date of a given observation night (a sinusoidal-like function with its maximum reaching 293 K in January and with a minimum at 273 K in July).

3. Two methods of analysis

Two methods to determine the telescope pointing capabilities were recently developed. The first method automatically searches for the star signals in the background data. The central time of the signal (T_{signal}) is defined as the central point of the signal plateau (see Fig. 5). In turn, the signal is assumed to be produced by the star whose position is nearest to the pixel center. The star position is calculated at the central time of the detected signal and the difference between this calculated value and the nominal direction of the pixel's center is identified as the pixel offset. From the star's transit through a given pixel, a pointing direction of this pixel is derived. From each estimated pixel direction a pointing direction value of the camera optical axis is determined and used to calculate the overall offset of the camera. We call it the *single pixel method*.

The second method is somewhat different. We look for the optimization of the entire trajectory of a bright star across the camera and we identify the time of transit of this star between pixels. Then we look for time differences between expected (computed) times of transit, with some given offset for the whole camera, and transit times found in data. We go through the matrix of all possible camera center offsets, in a range in azimuthal coordinates, and then we select the optimum offset with the smallest difference between expected and identified times of transits. The typical trajectory of a star consists of about 20 transits between pixels and the whole star track is optimized at once. Many (~100) such tracks are analyzed and optimized for each camera. The resulting offset of the given camera is then finally calculated as the weighted average of these found offsets. We call it the *star track method*.

The two analysis programs were designed to process automatically the background data. The initial idea was to select some basic criteria and data file, run the program and directly obtain the elevation and azimuthal offset of the camera. We also processed several nights' data including the camera rotation as a parameter and we found that rotation offsets were negligible. This is in agreement with the alignment method of the camera, where it was possible to measure (and remove) the camera tilt very precisely.

To achieve such a goal, the methods were designed to:

- automatically find and select the brightest star traversing each telescope field of view during the selected nights;
- read the variance data from background files for each pixel at each analyzed camera, together with timestamp;
- identify star signals within background data and compare them with computed expected signals;
- determine the pointing direction of each camera axis through the analysis of the differences found between the data and the expected signals.

More detailed description of both methods follows below.

4. Single pixel method

The logical scheme of our procedure can be summarized basically in the following four steps:

(1) search for signals in the baseline variance data;
(2) find the stars that give origin to the signals found in (1);
(3) for each identified signal, determine a pointing value of the telescope's optical axis;
(4) determine the pointing of the telescope's optical axis from all the calculated values.

Steps (1)–(3) are repeated every night of the period under analysis (January 2004–October 2004 in this case) while step (4) is done at the end, when all the data taking period has been analyzed. In the following paragraphs each step of the procedure will be described.

4.1. Search for star signals in the baseline variance data

The sky background light varies from night to night and, in a single night, it may change within a few hours (Fig. 8). To overcome this inconvenience we have implemented two different methods: the Time-Over-Threshold (TOT) and the Slew-Rate (SR) algorithms. Their aims are to extract the signals from the variance data and to find their central time T_{signal}, i.e. the middle time of the associated plateau.

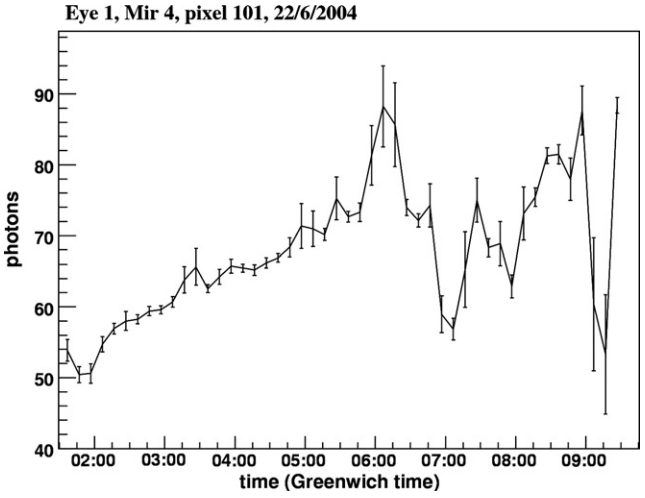

Fig. 8. Los Leones, telescope 4, pixel 101. Plot of the pixel variance as a function of time during the night 22/6/2004. The variance values are averaged every 10 min and converted to photons at the diaphragm.

In the TOT method we first calculate the mean value of the variance baseline, $\bar{v}$, and its RMS value, σ, in a time window of 2 h. If a star enters into a pixel's FOV, the background noise and the variance of this pixel will increase in a time range of 4–15 min depending on the star declination. Therefore, if a set of variance points is $v_i > \bar{v} + 3\sigma$ in this typical time range, a signal is identified and the pixel center is assumed to be pointing to the star direction at time T_{signal}.[5] The absolute pointing direction of each pixel is obtained transforming the equatorial coordinates of the star (right ascension and declination) at T_{signal} to the local coordinate system (elevation and azimuth).

The second method used to extract signals from variance data, the Slew Rate algorithm (SR), is a sort of derivative method. We calculate the increment of the variance between two separated points, $\delta = \Delta v/\Delta t = (v_i - v_j)/(t_i - t_j)$ every 4 *samplings points* (2 min) during the entire night. Positive and negative consecutive values of δ, within 4–15 min, will therefore correspond to the leading and trailing edges of a star signal. As for the first method, if a star signal is found, the pixel center is assumed to be pointing to the star direction at time T_{signal}. A schematic plot of the two methods is shown in Fig. 9 in the ideal signal case, while in Fig. 10 the real case is shown.

The variance signal in Fig. 10a has been converted into a number of photons at the diaphragm using the calibration constants obtained with the absolute calibration system [24,25], with which the detector response is measured using a large homogeneous diffuse light source with very precisely known light flux.

These two methods are complementary in the sense that their efficiencies depend on the signal shape and the background trend. The first method works better than the second one if the baseline is highly variable, but it is worse for small signals. As shown in Fig. 10 both methods work fine for high and clear signals.

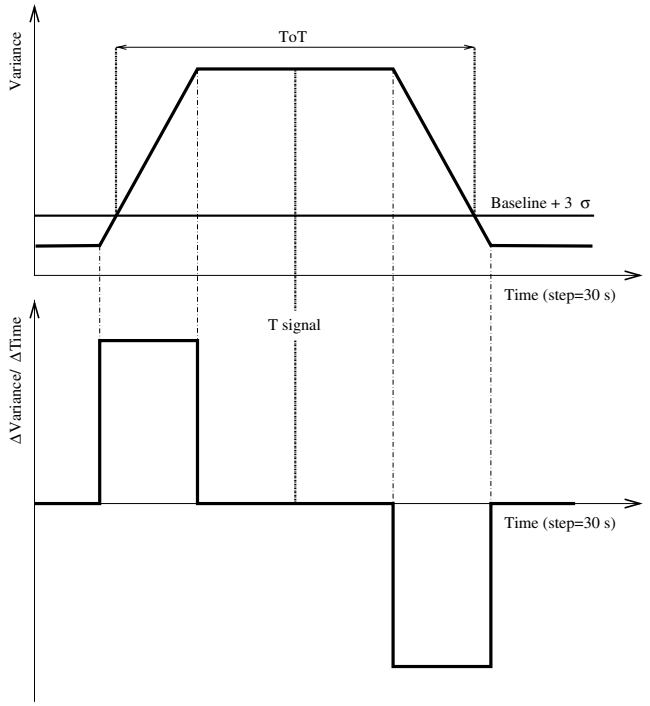

Fig. 9. Time-over-Threshold (ToT) scheme above, and Slew-Rate (SR) scheme below.

4.2. Star identification

Once all the signals has been found in the background variance data, we search for bright stars traversing the field of view of the camera during the night analyzed. For each star we compute the time at which the star entries and exits each pixel FOV. We defined these times as the first and last times at which the star spot is fully contained in the pixel FOV.[6] Once we have computed the stars time, we can identify the stars responsable of the signals founded in the background variance data through a time comparison. Transforming the equatorial coordinates of the star (right ascension and declination) at T_{signal} to the local coordinate system (elevation and azimuth) we obtain an estimate of the pixel pointing direction for each identified signal. As the camera has a rigid and defined structure (Section 2.1), we can determine a pointing direction value of the camera optical axis from each of these estimated directions. When the observation time is long, many signals could be found in a single pixel. Therefore, we will have as many telescope pointing estimations as signals found in the analyzed period. The statistical error in the determination of the camera pointing could be improved by analyzing the largest number of nights as possible.

[5] In practice, ideally, the star direction corresponds to the point nearest the pixel's center. As we only consider spots fully contained in the pixel (Section 4.2), the difference is smaller than ≈0.25°.

[6] In this way, we only consider spots fully contained in the pixel.

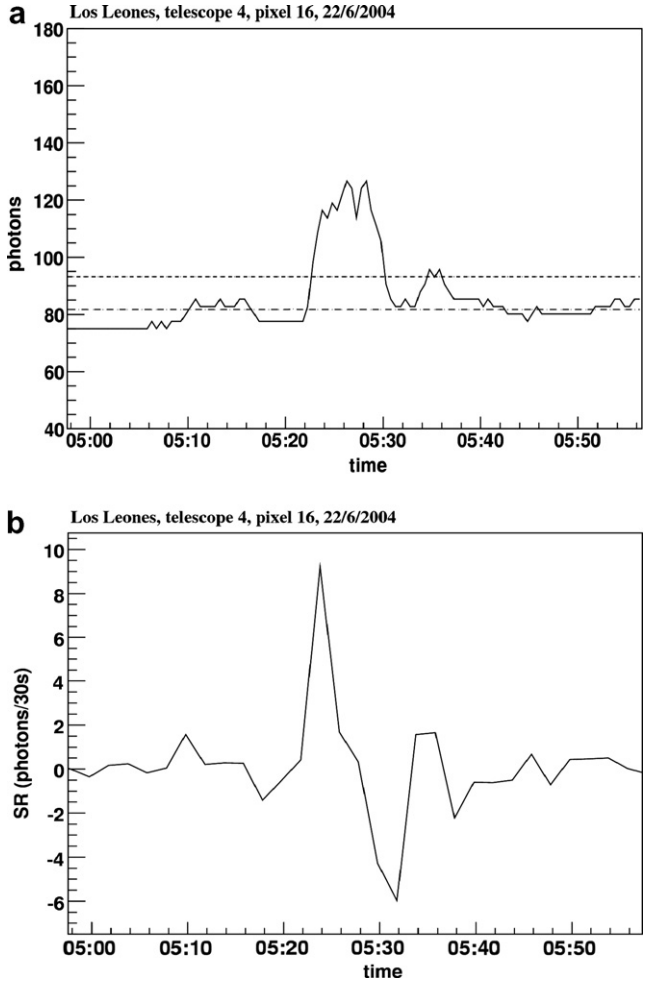

Fig. 10. Los Leones, telescope 4, pixel 16, 22 June 2004 (UTAle): signal of Beta Lyrae (U mag = 2.85). (a) The variance signal, converted to photons at the diaphragm, is shown; the dashed lines indicates the mean value and the mean value $+3\sigma$ of the background noise. (b) The derivative of the signal is plotted.

4.3. Determination of the camera pointing

As explained in the previous section, from each estimated value of the pointing of each pixel we are able to calculate the elevation and azimuth of the camera axis by simply inverting the formulas (1) and (2) given in Section 2.1.[7] Once a first estimation of the pointing has been calculated, we set the elevation and azimuth of the camera axis to the estimated values and we calculate the new pixel coordinates; the process is so repeated from step (2) to (4). The number of iterations required is evaluated through the number of star signals identified. The analysis of the data shows that the maximum number of iterations required is equal to 3.

[7] Actually the camera position has 5 degrees of freedom, the three-dimensional position of its centerpoint and rotation around two independent axis. However, no significant rotation offset has been found.

Histograms of the calculated camera offset in elevation and azimuthal angle for some telescopes at Los Leones and Coihueco are shown in Figs. 11 and 12.

5. Star track method

The procedure of the method can be summarized in the following steps:

- Automatically find and select the brightest stars with sufficiently long trajectories across the camera during the selected night.
- Read the variance data from background files for each pixel at the analyzed camera, together with timestamp.
- Identify star signals within background data and compare them with computed expected signals.
- Shuffle with the camera's center position and try to optimize the differences found between the data and the expected signals.

5.1. Star tracks and transits between pixels

We can follow the star traversing the camera FOV and quite easily identify the pixels with increased signals due to star light. An example of several such star tracks is shown in Fig. 13.

We can identify the instants when the star spot center (SSC) moves from one pixel to an adjacent one. These times of SSC transit are crucial for our analysis. We expect that before this time the variance of the former (''old'') pixel is higher than that of the latter (''new'') pixel and that, after this time, the variance of the ''old'' pixel is lower than the variance of the ''new'' pixel. We note that by tracking SSCs we naturally solve the problem of the star image projected simultaneously onto 3 pixels. The SSC moves across the pixel boundary from one specific pixel to a neighboring one.

Knowing the precise position of a given star on the sky as well as the correction due to SSC offset, we transform this position to camera coordinates and compute the instant when the star is crossing the boundary between hexagonal pixels. We compute such instants for all illuminated camera pixels and we identify the times of transits of the spot center for the whole star track across the camera.

5.2. Star track optimization

As described above, we are able to compute both the trajectory of SSC across the given FD camera and the transit time of the SSC from pixel to pixel. Furthermore, we are able to identify these transits between pixels in the real background data.

We analyze the data from about 180 s ahead of the expected transit to about 180 s after the expected transit. During this period, we check if there is a greater variance value for at least two consecutive samples on the former

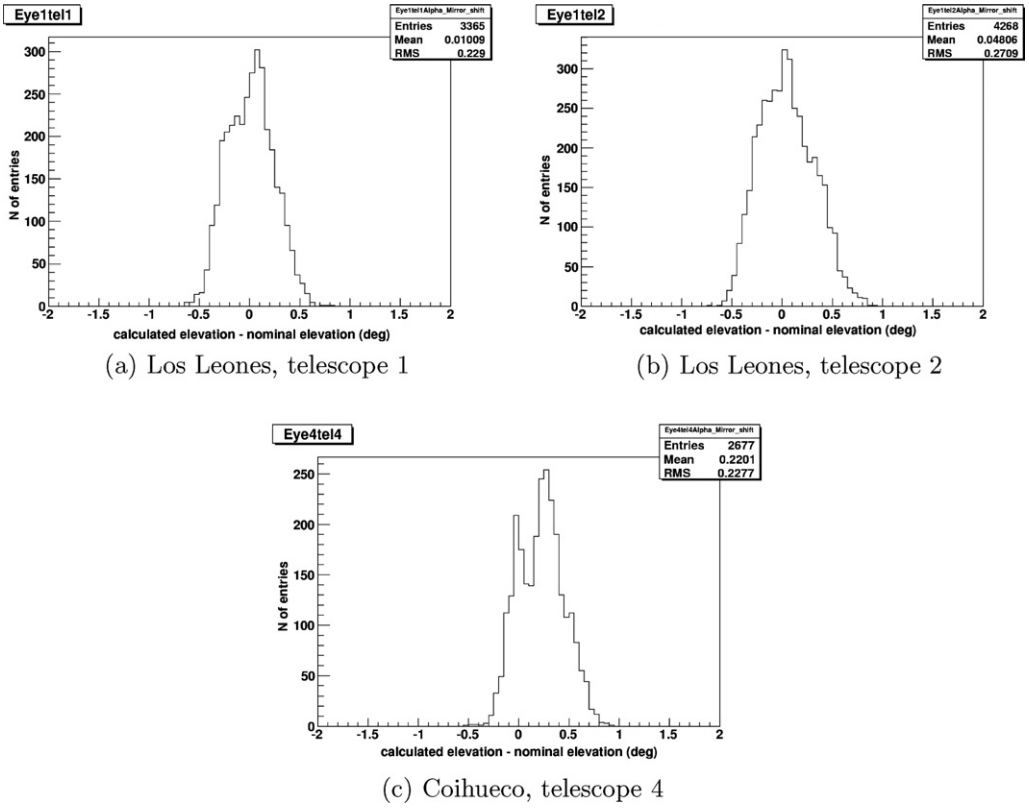

(a) Los Leones, telescope 1 (b) Los Leones, telescope 2

(c) Coihueco, telescope 4

Fig. 11. *Single pixel method*: histograms of the differences between the reconstructed and nominal values of the elevation angle of the telescope optical axis. The results were obtained using the data of the entire period analyzed (Sections 6.2 and 7.1, Table 1).

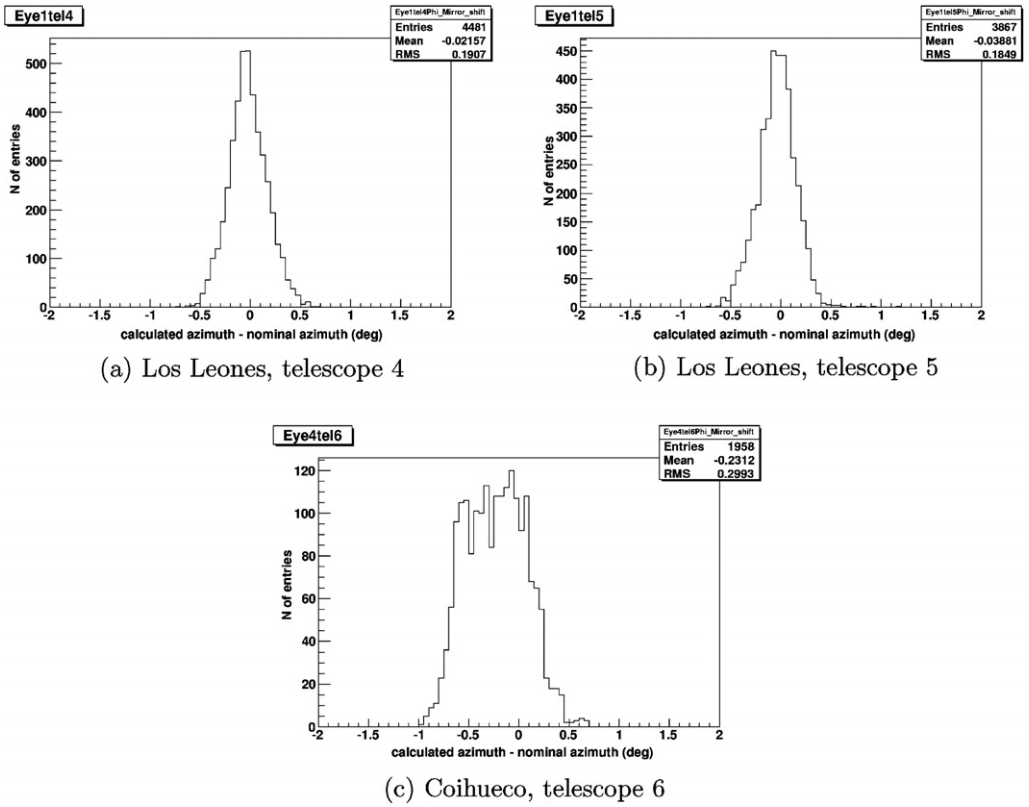

(a) Los Leones, telescope 4 (b) Los Leones, telescope 5

(c) Coihueco, telescope 6

Fig. 12. *Single pixel method*: histograms of the differences between the reconstructed and nominal values of the azimuthal angle of the telescope optical axis. The results were obtained using the data of the entire period analyzed (Sections 6.2 and 7.1, Table 1).

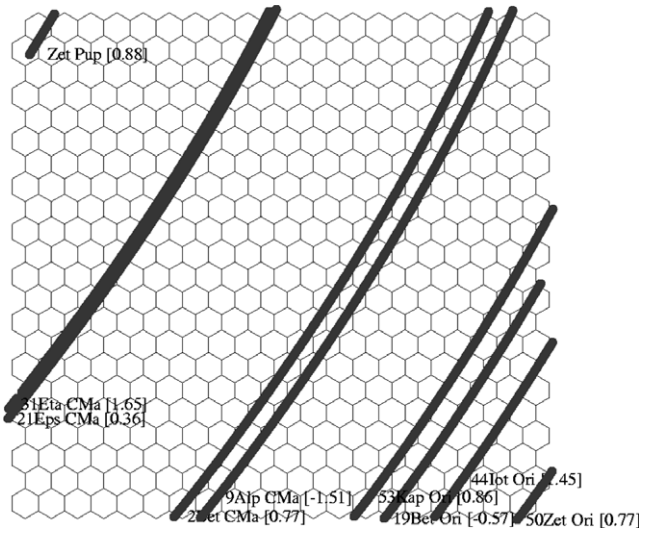

Fig. 13. Typical set of star tracks. Imaged tracks are for the Los Leones FD camera, bay 1, for the night of November 13th/14th 2004 (21 h UT – 07 h UT). Only the stars brighter than second magnitude were plotted.

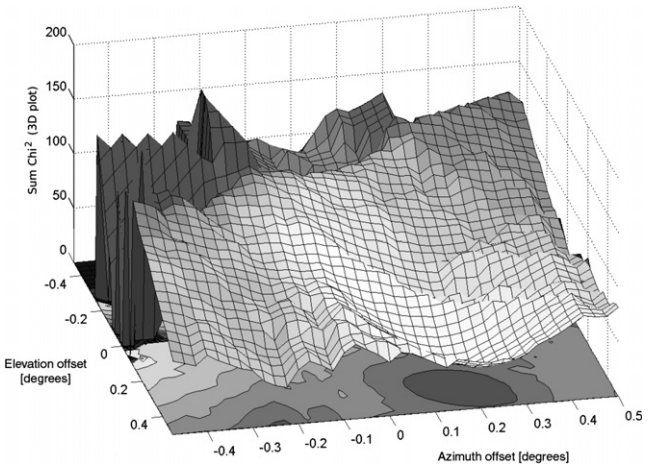

Fig. 14. Star track optimization, graph for one chosen star (β Ori). The contour plot on the bottom plane shows that the optimized offset is about 0.2° for azimuth and about 0.3° for elevation. For details, see Section 5.2.

"old" pixel than on the latter "new" pixel. For both consecutive samples, the variance on the "old" pixel has to be greater than the variance on the "new" pixel at least by 1 (ADC count)^2.[8] Such a period has to be immediately followed by two consecutive data samples, where the situation is opposite, i.e. a star already traversed to a "new" pixel. So, these two consecutive signals on the "new" pixel have to be greater at least by 1(ADC count)^2 than the signal in the "old" pixel. The star transit is then expected to occur between times of this intensity switch. The exact time is analytically computed as the crossing of interpolated signals of "old" and "new" pixels. The signal values surrounding the instant of this transit are used for interpolation.

We then have both predicted times of transits and also detected times of transits in the data for the whole track. For these times we can easily calculate $\sum\chi^2$ and use it as our main optimization parameter. Having this initial value we can start shuffling with the camera center on the regular grid.

We used shuffling $\pm 0.5°$ around the nominal center of the camera on the regular grid with steps of 0.025°. Doing this, we are looking for the least average time offset for the whole track. During shuffling we compute the new times of transits between pixels and we can even find completely new transits between previously not illuminated pixels. As the second parameter we also check the number of transits detected in background data, which of course could be larger than the starting number of detected transits, but should not be much smaller than the initial one. In practice, we use a condition which rejects the new resulting shuffled tracks if the new trajectory would diminish the number of transits by more than 4.

The typical results of one star track optimization are shown in Fig. 14, where all time differences from the shuffling grid are plotted.

In Fig. 14, the contour plot on the bottom plane shows that the optimized offset is about 0.2° for azimuth and about 0.3° for elevation. The darker areas indicate the regions with smaller differences between detected times of transits and predicted times of transits; lighter areas are for greater time differences. The 3D plot above shows the same thing, the deepest valley is for the smallest difference of time offset. However, the coloring is different, light colors indicate a large number of detected star transits, dark colors indicate a very low number (or even zero) of successfully detected transits. Practically, we are looking for some sort of anti-correlation for regions with low $\sum\chi^2$ and a high number of pixels of the star track.

Histograms of the computed camera offset for some telescopes at Los Leones and Coihueco are shown in Figs. 15–17.

5.3. Analysis of lightcurves

We can track some bright stars through a given camera and read out the values of variances of the pixels that are closer than 0.5° to the center of the star which means the values between 1 and 3 pixels. We subtract the "sky background" value for each pixel, calculated as the average of signals of a given pixel some time before and after the star transit. (We generally used averages of 15 min before and 15 min after the period of time, when the star was traversing

[8] The typical variance difference between two illuminated neighboring pixels for used bright stars (with $U_{\mathrm{mag}} < 2$) is usually much greater. During the development of our code, we tested different (larger) minimal differences of variance and did not find any significant changes in our results. Finally, we used this relaxed condition (1(ADC count)^2 difference), which proved to be only a little more sensitive for signal detection in the lowest part of the camera. However, we found that the condition of having the "old" pixel brighter for two samples and, immediately after that, fainter for the next two samples is strong enough to exclude random fluctuations even for this sensitive limit of 1(ADC count)^2 difference.

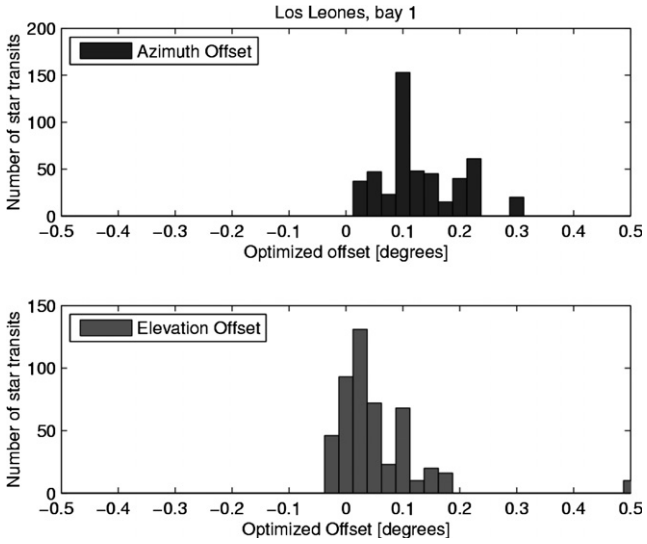

Fig. 15. Los Leones, telescope 1: histograms of the optimized camera offset for elevation and azimuth angles obtained with the *star track method*. The results were obtained using the data of the entire period analyzed (Section 6.2).

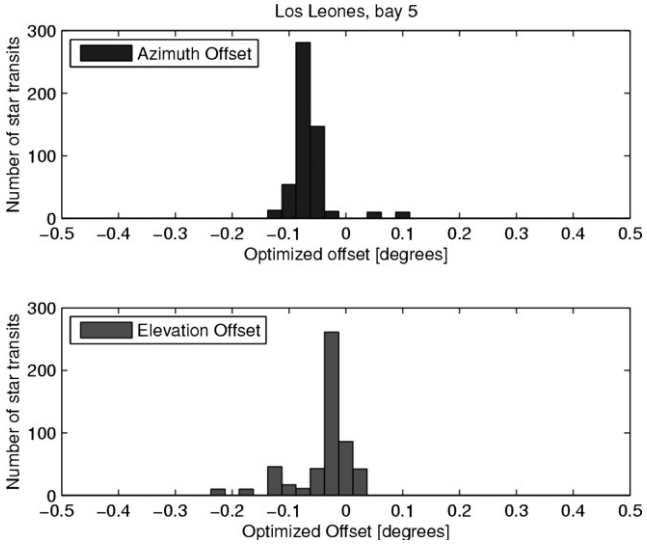

Fig. 16. Los Leones, telescope 5: histograms of the optimized camera offset for elevation and azimuth angles obtained with the *star track method*. The results were obtained using the data of the entire period analyzed (Section 6.2).

the pixel.) The sum of corrected signals from all contributing pixels can then be plotted as a function of star altitude.

The sum of the signal from all the pixels illuminated by the spot of the star should be almost constant (or slowly growing with altitude); there could likely be smaller bumps due to the influence of reflective plastic inserts or changes due to sudden shifts in atmospheric extinction. However, such results are not obtained for the original directions of the cameras. An example for the bay 4 at Coihueco is shown in the upper plot of Fig. 18.

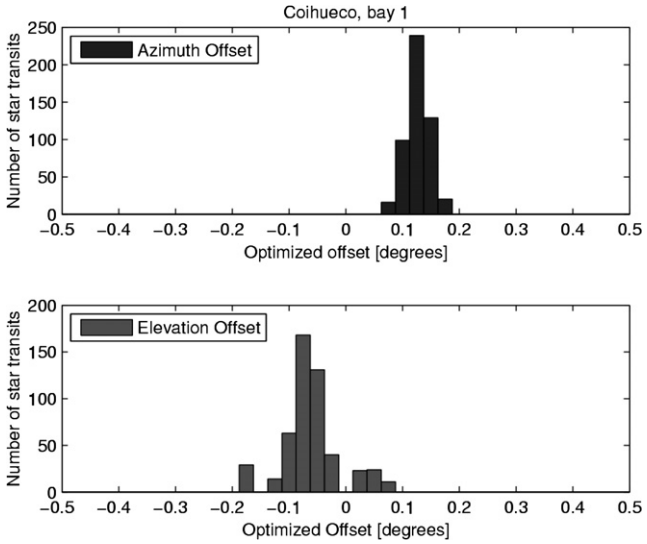

Fig. 17. Coihueco, telescope 1: histograms of the optimized camera offset for elevation and azimuth angles obtained with the *star track method*. The results were obtained using the data of the entire period analyzed (Section 6.2).

We can see that for some positions of the star image on the camera we are not even observing the correct pixels (not really the ones containing a star signal at that time) and therefore, we observe a significant signal drop.

For the optimized position of the camera (with the pointing direction found with this method) the situation is generally much better, and the resulting curve is approximately a straight line (lower part of Fig. 18). This could be taken as a proof that our results indicate real offsets of the camera centers.

6. Analyzed data

After July 2004 the Observatory started to operate with 12 telescopes, 6 in the FD site of Los Leones and 6 in Coihueco. Since April 2005, the telescopes of the Los Morados site have been installed.

The two procedures described in the previous sections have been applied to calculate the pointing of the 12 telescopes of the fluorescence detector installed at Los Leones and Coihueco. The data used and the results obtained with the two methods are described in the following sections.

6.1. Star catalogue used

As the two described methods were developed independently, two different star catalogues were used. Because of the presence of the UV filter at each telescope's aperture, we take into consideration only those stars of sufficient brightness in the U spectral band.

For the *single pixel method* analysis we use the UBV Photometry of Bright Stars catalogue [26] that includes 3777 stars with U magnitude lower than $U_{\mathrm{mag}} = 8$. We defined $U_{\mathrm{mag}} = 3$ as the U magnitude of the faintest star

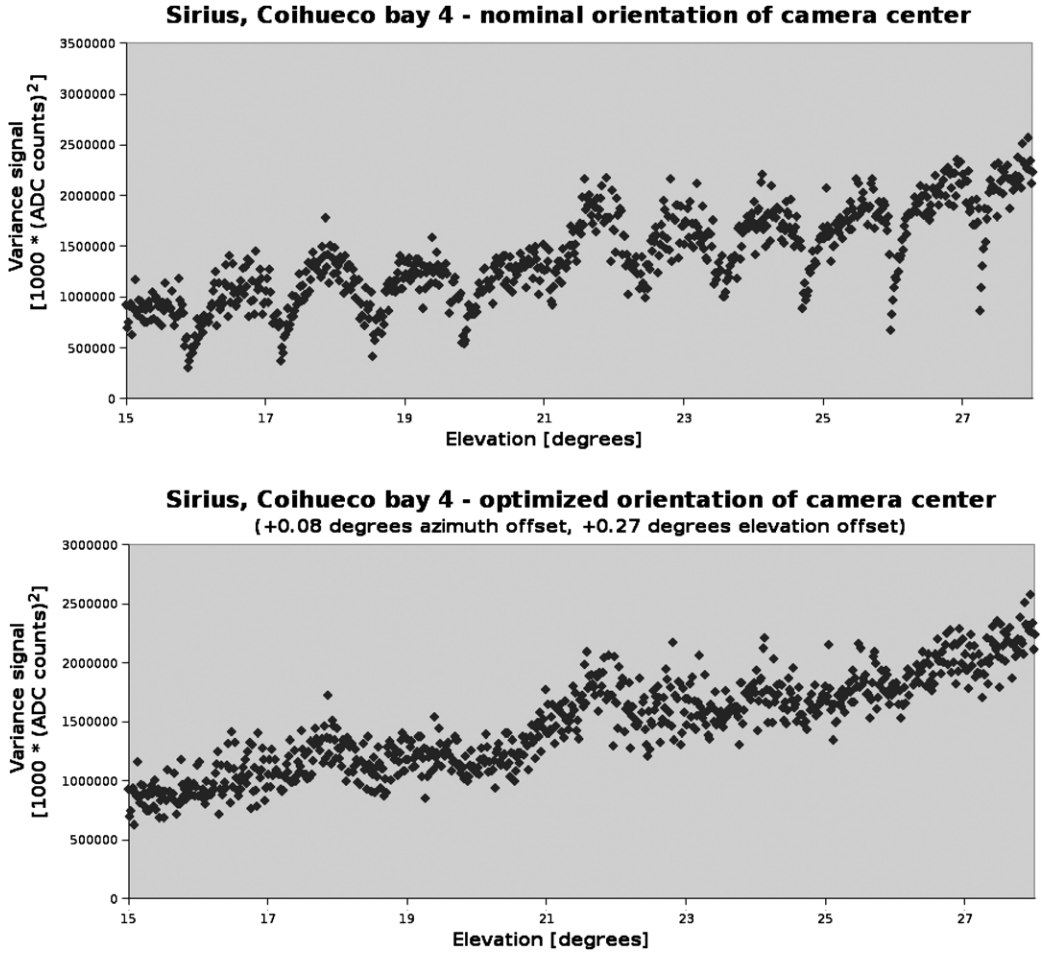

Fig. 18. Comparison of lightcurves for original and optimized camera positions of Coihueco bay 4. The data used for the plot are from November 14th 2004 which were taken with a higher sampling rate of 0.2 Hz (instead of the ordinary 0.03 Hz sampling rate).

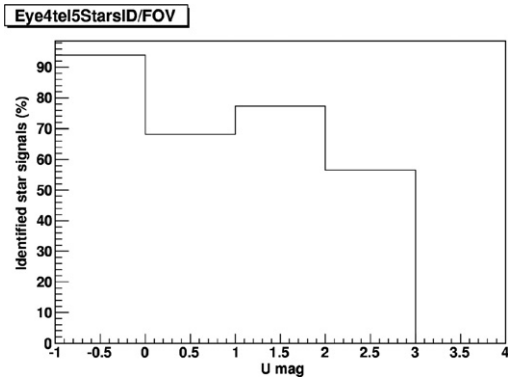

Fig. 19. Coihueco, telescope 5. Histogram of the percentage of star signals identified in the whole period analyzed (Table 1) as a function of U magnitude.

to be accepted.[9] In Fig. 19, the percentage of star signals identified in the whole period analyzed (Table 1) as a function of U magnitude shows the efficiency of our method. We are able to find and identify about 56% of the signals left by stars of 2–3 U mag traversing the telescope's FOV. For the transformation of star coordinates we used the `libnova` library.[10]

For the *star track method* analysis we used the Bright Star Catalogue (BSC) [27]. This catalogue contains basic astronomical and astrophysical data for all 9096 stars which are brighter than 6.5 magnitude. Using available data for each star we computed its magnitude in Johnson's U-band and we sorted the catalogue according to star brightness in the U-band and cut off all unnecessary information. If we want to analyze the entire star tracks across the camera, we have to concentrate on those bright stars which are visible also in the lower part of the camera. In fact, when the image of a star is projected on a pixel, the variance increases. The amplitude of this increase depends on the pixel position on the camera because the lower pixels suffer much more prominent losses due to atmospheric extinction. From empirical analysis it follows that for stars

[9] This catalogue contains 146 stars brighter than 3 U magnitude, 54 stars brighter than 2 U magnitude, 18 stars brighter than 1 U magnitude, 3 stars brighter than 0 U magnitude for the whole sky.

[10] http://libnova.sourceforge.net.

Table 1
"Single pixel method", Los Leones and Coihueco: rate of signals identified for the entire period analyzed (January–October 2004)

Telescope	Number of nights	Number of hours	Hours per night	Number of signals	Rate (signals/h)	Number of stars
Los Leones: rate of stars signals identified						
1	70	388	5.54	3365	8.7	36
2	71	407	5.73	4268	10.5	29
3	119	680	5.71	5832	8.6	32
4	110	636	5.78	4481	7.0	26
5	109	628	5.76	3867	6.2	25
6	115	633	5.50	5664	8.9	30
Coihueco: rate of stars signals identified						
1	34	183	5.38	787	4.3	16
2	77	463	6.01	1242	2.7	24
3	96	575	5.99	9160	15.9	58
4	35	189	5.40	2677	14.2	24
5	33	188	5.70	3582	19.1	25
6	31	164	5.29	1958	11.9	25

For details see Section 7.1.

fainter than fourth magnitude the signal increase is almost negligible (e.g. only about 1(ADC count)^2 for star ρ Gem (U magnitude equal to 4.47) at altitude 3.5°). Therefore, we concentrated only on the brightest stars in the sky, i.e. the stars which are brighter than magnitude 2.0 in the U filter,[11] which have significant offsets from sky background also in the lower part of the camera.

6.2. Processed data

The *single pixel method* and the *star track method* have been applied respectively to data acquired in the period January–October 2004 and April–November 2004. As the telescopes were not installed at the same time, the pointing of the 12 telescopes installed at the Los Leones and Coihueco was reconstructed with different amounts of data, proportional to the time each telescope acquired data.

For the *single pixel method* procedure, no selection of nights has been applied, with the exception of an acquisition time duration longer than 1 h. In the analyzed period, telescopes 3–6 at Los Leones operated around ~9 months while telescopes 1 and 2 operated ~3–5 months. On the other hand, at Coihueco, telescope 2 and telescope 3 operated around 8 months while the others operated around 3 months in the mentioned period. These periods must be reduced because of the duty cycle limited to ≈10%, as data are acquired only in moonless nights or nights with at most a quarter moon.

For the *star track method* procedure, based on times of transits of the light spot between pixels, we tried not to bias data with star signals diminished or otherwise modified by clouds moving through the studied pixel. Therefore, we tried to select only very clear, cloudless nights. For this reason, we used the cloud monitor database [28] and manually selected only completely clear nights of a given period. Because Coihueco was fully operational only since June 2004, the choice of suitable nights was more limited than for Los Leones: only 10 nights for Coihueco and 15 nights for Los Leones survived this cut.

[11] There are 6 stars brighter than zero magnitude, 24 stars brighter than first magnitude and 63 stars brighter than second magnitude in the U band for the whole sky.

7. Pointing results

In this section, we present the results obtained applying the two procedures to the background data acquired in 2004. The obtained pointing directions of the optical axis of the FD telescopes are compared with the nominal values specified in the Auger Offline reconstruction code.

The offsets obtained by the two methods are generally larger for elevations of the camera than for the azimuthal settings. This is basically what was expected from the camera alignment methods. The differences of our results and the nominal values for the FD are less than 0.3° and for the majority of telescopes are less than 0.1°.

7.1. Single pixel method: results

The total number of nights and the corresponding total number of hours analyzed (columns 2 and 3) for the FD sites at Los Leones and Coihueco are shown in Table 1, as well as the rate of identified signals (column 6), for the entire period analyzed (January–October 2004). The total number of signals identified and the number of stars analyzed are also shown in columns 5 and 7. Taking into account the effective observation time, the rate of identified signals varies from ~6.2 to ~10.5 signals/h for the Los Leones site, and from ~2.7 to ~19.1 signals/h for the Coihueco site. If the number of stars (with $U_{\mathrm{mag}} < 3$) passing through the field of view of each telescope during the whole analyzed period is taken into account, the rate of signals varies from ~0.24 to ~0.36 signals/(h star) for the site at Los Leones, from ~0.11 to ~0.76 signals/(h star) for the site at Coihueco.

Table 2
"Single pixel method", results for Los Leones and Coihueco: elevation and azimuthal angle of the optical axis

Telescope number	Elevation		Azimuth		Number of signals
	Δ_{elev} (deg)	RMS_{elev} (deg)	Δ_{az} (deg)	RMS_{az} (deg)	
Los Leones					
1	0.01	0.23	0.08	0.36	3365
2	0.05	0.27	−0.01	0.33	4268
3	0.00	0.35	−0.03	0.30	5832
4	0.10	0.46	−0.02	0.19	4481
5	0.03	0.43	−0.04	0.18	3867
6	−0.04	0.35	−0.06	0.29	5664
Coihueco					
1	0.05	0.49	0.12	0.34	787
2	0.08	0.36	−0.02	0.39	1242
3	0.00	0.28	−0.05	0.41	9160
4	0.22	0.23	−0.10	0.33	2677
5	0.14	0.27	−0.07	0.33	3582
6	0.24	0.35	−0.23	0.30	1958

The differences between the reconstructed values and the specified ones are shown with their RMS (Section 7.1).

Detailed results of the pointing values obtained with the *single pixel method* are shown in Table 2. Columns 2 and 4 in the table show the differences (deg) between the results obtained with our own analysis and the pointing values specified in the Pierre Auger Observatory database, used for the shower reconstruction. Columns 3 and 5 contain the RMS of the distributions of the elevation and azimuth values in the determination of the optical axis direction. The total number of identified signals in the entire period analyzed is also indicated (column 6).

As can be seen from the RMS values and from the positions of the telescopes (Fig. 1), the *single pixel method* is more sensitive to shift of the camera parallel to the star tracks. For example, telescope 5 at Los Leones, which points to the North where stars move almost horizontally, presents a smaller RMS in the azimuthal angle than telescope 2 at Los Leones, which points to the East where stars are rising.

Table 3
"Star track method", results for Los Leones and Coihueco: the differences (deg) of reconstructed (optimized) minus nominal values for the cameras are shown (Section 7.2)

Telescope number	Elevation		Azimuth	
	Δ_{elev} (deg)	$Error_{elev}$ (deg)	Δ_{az} (deg)	$Error_{az}$ (deg)
Los Leones				
1	0.05	0.08	0.13	0.07
2	0.06	0.12	0.00	0.10
3	−0.03	0.07	−0.07	0.05
4	0.06	0.08	−0.09	0.06
5	−0.04	0.05	−0.07	0.03
6	−0.16	0.08	−0.10	0.05
Coihueco				
1	−0.06	0.05	0.13	0.03
2	0.19	0.05	0.07	0.04
3	0.15	0.05	−0.04	0.09
4	0.27	0.06	−0.07	0.07
5	0.17	0.12	−0.04	0.10
6	0.23	0.03	−0.22	0.05

7.2. Star track method: results

The results of our analysis are summarized in Table 3.

The final offset of each camera was computed as the weighted average of all optimal offsets associated with successfully identified star tracks for the sample of selected nights. The track was considered as successfully identified if it was uninterrupted and if it contained more than 9 transits between pixels. Shorter tracks were not used. The optimized camera offset was computed for each track and weighted with the number of detected transits for this optimized track. The statistical error, also shown in Table 3, was then computed as a weighted standard deviation of individual track offsets.

7.3. Comparison

In this section, we present a comparison of the results obtained with the two methods.

The actual differences (deg) between the offsets found with the two methods are given in Table 4. For each method (indicated as *Single* for the *single pixel method* and *Track* for the *star track method*), the differences between reconstructed and nominal values are shown. The third (boldface) column for each bay contains the difference of the values obtained with the two methods.

The accuracy in the determination of the camera pointing obtained with the two method is different; while the *single pixel method* has the advantage of better statistics, the *star track method* has a better resolution.

As can be seen from the histograms in Figs. 11, 12, 15, 16 and 17, the distributions are narrower and the respective errors are smaller for the *star track method*. This can be due to several reasons. The *star track method* uses only selection of clear nights that reduces biases due to clouds and bad weather, which very likely influenced the results of *single pixel method*. Also, the use of the full star track with

Table 4
Comparison of the results obtained with the two methods

	Bay 1			Bay 2			Bay 3		
	Track	Single	Diff.	Track	Single	Diff.	Track	Single	Diff.
Los Leones									
Azimuth	0.13	0.08	**0.05**	0.00	−0.01	**0.01**	−0.07	−0.03	**−0.04**
Elevation	0.05	0.01	**0.04**	0.06	0.05	**0.01**	−0.03	0.00	**−0.03**
	Bay 4			Bay 5			Bay 6		
	Track	Single	Diff.	Track	Single	Diff.	Track	Single	Diff.
Azimuth	−0.09	−0.02	**−0.07**	−0.07	−0.04	**−0.03**	−0.10	−0.06	**−0.04**
Elevation	0.06	0.10	**−0.04**	−0.04	0.03	**−0.07**	−0.16	−0.04	**−0.12**
	Bay 1			Bay 2			Bay 3		
	Track	Single	Diff.	Track	Single	Diff.	Track	Single	Diff.
Coihueco									
Azimuth	0.13	0.12	**0.01**	0.07	−0.02	**0.09**	−0.04	−0.05	**0.01**
Elevation	−0.06	0.05	**−0.11**	0.19	0.08	**0.11**	0.15	0.00	**0.15**
	Bay 4			Bay 5			Bay 6		
	Track	Single	Diff.	Track	Single	Diff.	Track	Single	Diff.
Azimuth	−0.07	−0.10	**0.03**	−0.04	−0.07	**0.03**	−0.22	−0.23	**0.01**
Elevation	0.27	0.22	**0.05**	0.17	0.14	**0.03**	0.23	0.24	**−0.01**

Differences between the reconstructed and nominal values (deg) are shown for both the methods. The differences of the values obtained with the two methods are shown in the third column.

certain minimum length (10 pixels) adds another quality constraint that is not present for *single pixel method*. Finally, the *single pixel method* suffers from the fact that stars typically do not go right through the center of each pixel and that the middle of the plateau is not necessarily the point of closest approach of the star to the pixel center, especially if the spot size is not spherical.

Both methods are then influenced by the unremovable factor of sampling (equal to 30 s). Any star covers a distance of 0.125° in 30 s, therefore, we cannot see the real time of transit between pixels or the time of the closest approach to the pixel center, and so we are biased by this time sampling. We can assume the magnitude of this error to be the same as the standard deviation of the uniform distribution on the interval $[0°, 0.125°]$ that is equal to $0.125°/\sqrt{12} = 0.04°$.

Another independent check of the telescope pointing can be obtained using laser shots from the Central Laser Facility (CLF) [28]. The CLF is used to emulate showers for atmospheric monitoring and calibration purposes. Independent studies were performed by two Auger groups. The first group analyzed the vertical shots for a selected telescope (bay 4 at Los Leones) and concludes that the telescope's pointing is consistent with our own results. The second group analyzed inclined laser shots for several selected bays at the Coihueco site. The reconstructed shower parameters better match our pointing values rather than the nominal ones (Fig. 20).

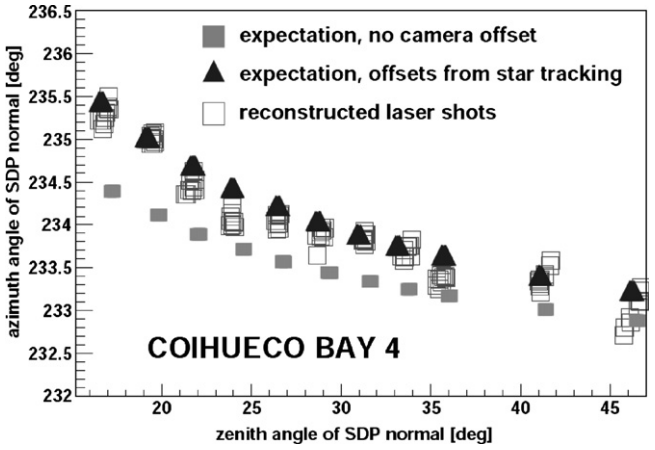

Fig. 20. CLF results. The plot shows the reconstructed azimuth and zenith angle of the normal to the shower-detector-plane (SDP) of inclined laser shots. The expected parameters for the nominal telescope pointing direction (no offsets) and for our pointing results are shown.

8. Summary and conclusions

We described two methods to determine the pointing of the optical axis of the fluorescence detector telescopes at the Pierre Auger Observatory. The two methods described, called the *single pixel method* and *star track method*, are based on the capability of the fluorescence detector (FD) to be sensitive to the variance signals left by stars traversing the telescope field of view. The identification of the star signals provides a powerful tool to check and monitor the telescope alignment.

The two procedures were applied to the data acquired in 2004 for all 12 telescopes installed at the FD Los Leones and Coihueco sites, providing compatible sets of pointing direction results. The differences between the results obtained with both procedures and the nominal values specified for the FD are less than 0.3° and for the majority

of telescopes are less than the precision of the procedure to set the pointing of the telescopes, which is 0.1°.

Moreover, the results obtained with independent studies using both vertical and inclined laser shots are consistent with our own results, confirming the validity of our methods.

Knowledge of correct pointing directions is an essential ingredient in the Auger Observatory's unique hybrid event reconstructions and for all comparisons with SD geometric reconstructions of those same events. Our methods will strengthen these analyses. Using our above described methods we are now also prepared to easily monitor the long-term stability of the measured pointing directions and to use our pointing values to improve the precision of the hybrid reconstruction.

Acknowledgements

The authors from Institute of Physics, Prague, Czech Republic were supported by the grant LC 527 of the Czech Ministry of Education, Youth and Sports of the Czech Republic and by the grant No. 202/06/P006 of Grant Agency of the Czech Republic.

We also thank Sergio Petrera and Greg Snow for their careful reading of the manuscript and for their extremely helpful and valuable recommendations. We also thank anonymous referee, whose comments significantly improved the clarity and stressed the message of the paper.

References

[1] K. Greisen, Cosmic ray showers, Annual Review of Nuclear and Particle Science 10 (1960) 63–108.

[2] J. Delvaille, F. Kendzicrski, K. Greisen, Spectrum and isotropy of EAS, Journal of the Physical Society of Japan 17 (Suppl. A-III) (1962) 76;
Proceedings of the International Conference on Cosmic Rays and the Earth Storm, 5–15 September, 1961, Kyoto. Volume: II1, Cosmic Rays., Physical Society of Japan, 1962.

[3] A.E. Chudakov, K. Suga, in: I. Escobar et al. (Eds.), Proceedings of Fifth Interamerican Seminar on Cosmic Rays, Laboratorio de Fisica Cosmica de la Universidad Mayor de San Andreas, La Paz, Bolivia, 2, 1962, p. XLIX.

[4] R.H. Hughes, J.L. Philpot, C.Y. Fan, Spectra induced by 200-keV proton impact on nitrogen, Physical Review 123 (1961) 2084–2086.

[5] A.N. Bunner, Ph.D. thesis, Cornell University, 1964.

[6] F. Kakimoto, E.C. Loh, M. Nagano, H. Okuno, M. Teshima, S. Ueno, A measurement of the air fluorescence yield, Nuclear Instruments and Methods in Physics Research A 372 (1996) 527–533.

[7] M. Nagano, K. Kobayakawa, N. Sakaki, K. Ando, Photon yields from nitrogen gas and dry air excited by electrons, Astroparticle Physics 20 (2003) 293–309, astro-ph/0303193.

[8] P.A. Sadowski et al., High Resolution Fly's Eye Collaboration, Geometry and optics calibration for air fluorescence detectors using star light, Astroparticle Physics 18 (2002) 237–248.

[9] Auger Collaboration, Technical Design Report, 2004, pp. 1–491.

[10] J. Abraham et al., Properties and performance of the prototype instrument for the Pierre Auger Observatory, Nuclear Instruments and Methods A 523 (2004) 50–95.

[11] M. Ambrosio, C. Aramo, F. Bracci, P. Facal, R. Fonte, G. Gallo, E. Kemp, G. Matthiae, D. Nicotra, P. Privitera, G. Raia, E. Tusi, G. Vitali, The camera of the Auger fluorescence detector, IEEE Transactions on Nuclear Science 48 (2001) 400–405.

[12] H. Bluemer, The Auger fluorescence detector prototype telescope, in: Proceeding of the 26th International Cosmic Ray Conference, Salt Lake City, 1999, p. 345.

[13] G. Borreani, N. Cartiglia, R. Cester, F. Daudo, A. De Capoa, M.A.L. De Oliveira, F. Marchetto, D. Maurizio, N. Pastrone, The fluorescence detector prototype for the Auger project: mechanical structure, optical system, and filter, IEEE Transactions on Nuclear Science 48 (2001) 406–410.

[14] H.O. Klages, H. Kleinfeller, E. Bluemer, R. Bollmann, J. Gumbsheimer, Optical components for the fluorescence detectors of the Pierre Auger experiment, in: Proceedings of the 27th International Cosmic Ray Conference, Hamburg, Germany, 2001, p. 764.

[15] G. Matthiae, The Pierre AUGER Observatory Collaboration, Optics and mechanics of the Auger fluorescence detector, in: Proceedings of the 27th International Cosmic Ray Conference, Hamburg, Germany, 2001, p. 733.

[16] C. Escobar, R. Sato, The performance of the corrector lenses for the Auger fluorescence detector, in: 29th ICRC, Pune, International Cosmic Ray Conference, vol. 8, 2005, p. 13.

[17] S. Argirò, D.V. Camin, M. Destro, C.K. Guérard, Monitoring DC anode current of a grounded-cathode photomultiplier tube, Nuclear Instruments and Methods in Physics Research A 435 (1999) 484–489.

[18] S. Argirò, D.V. Camin, P. Cattaneo, M. Destro, R. Fonte, R. Gariboldi, et al., The analog signal processor of the Auger fluorescence detector prototype, Nuclear Instruments and Methods in Physics Research A 461 (2001) 440–448.

[19] D.V. Camin, V. Grassi, F. Sanchez, V. Scherini, Use of star tracks to determine photocathode anisotropy of PMTs and absolute pointing of the Pierre Auger fluorescence detector telescopes, IEEE Transactions on Nuclear Science 51 (2004) 3034–3037.

[20] M. Kleifges, A. Menshikov, D. Tcherniakhovski, H. Gemmeke, Statistical current monitor for the cosmic ray experiment Auger, IEEE Transactions on Nuclear Science 50 (4) (2003) 1204–1207.

[21] R. Caruso et al., Pierre Auger Collaboration, Measurements of the sky photon background flux at the Auger Observatory, in: 29th ICRC, Pune, International Cosmic Ray Conference, vol. 8, 2005, p. 117.

[22] D. Dravins, L. Lindegren, E. Mezey, Atmospheric intensity scintillations of stars I.: statistical distributions and temporal properties, Publications of the Astronomical Society of the Pacific 109 (1997) 173–207.

[23] A. Meeus, Astronomical Algorithms, second ed., Willman-Bell, 1998, not cited.

[24] M.D. Roberts, Pierre Auger Collaboration, Calibration of the Pierre Auger Fluorescence Detector, in: Proceedings of the 28th International Cosmic Ray Conference, Trukuba, Japan, 2003.

[25] P. Bauleo et al., Pierre Auger Collaboration, Absolute calibration of the Auger fluorescence detectors, in: 29th ICRC, Pune, International Cosmic Ray Conference, vol. 8, 2005, p. 5.

[26] H.L. Johnson, R.I. Mitchell, B. Iriartes, W.Z. Wisniewski, UBV photometry of bright stars, Commun. Lunar & Planet. Lab. 4, 99, Table 9, 1966.

[27] D. Hoffleit, W.H. Warren Jr., The Bright Star Catalogue, fifth Revised Ed. (Preliminary Version), Astronomical Data Center, NSSDC/ADC, 1991.

[28] B. Fick, M. Malek, J.A.J. Matthews, J. Matthews, R. Meyhandan, M. Mostafá, M. Roberts, P. Sommers, L. Wiencke, The central laser facility at the Pierre Auger Observatory, Journal of Instrumentation 11 (2006) 3.